

Delayed-shot 3D Prestack Depth Migration

Yu Zhang, James Sun, Carl Notfors, Sam Gray, Leon Chernis and Jerry Young, Veritas DGC Inc.

Summary

We present a formulation for delayed-shot migration of marine data in 2-D (plane-wave sources) and in 3D (linear sources and planar sources). We present speedup factors for these delayed-shot migrations over common-shot migration, and we discuss some sampling theory issues associated with the formation of delayed-shot records. On both synthetic and real data examples, delayed-shot migration has produced images comparable to those from common-shot migration.

Introduction

The increasing demands of imaging complex geologic structures, for example beneath salt bodies, has led the industry to explore wave equation based prestack depth migration methods that do not suffer from the high frequency and multipathing limitations of Kirchhoff migration. However, common-shot migrations based on wavefield extrapolation are typically more computationally intensive, especially when 3D migrated common image gathers (CIG's) are output. This relative inefficiency has spurred researchers to seek various ways to speed up their wave-equation migration programs.

The computational cost of common-shot migration is roughly the cost of migrating a single shot record multiplied by the number of migrated shots. Reducing the number of shots, and consequently the number of migrations, is an obvious way to improve the total migration efficiency, although it is not obvious that simply decimating shots will allow one to maintain the fidelity of the migrated image. A different approach to reducing the number of shots without decimation is based on the linearity of the wave equation: a linear stacking of wavefields initiated at different shotpoints satisfies the same wave equation as each of the individual wavefields. Therefore, migration can be applied to the superposition of different shot records, allowing the total number of migrations to be reduced. This idea has led to the migration of phase-encoded shot records (Romero et al., 2000), in which a subset of all the shot records are linearly combined together by applying some phase functions chosen to reduce the cross-term artifacts. A specialization of this idea, called *delayed-shot migration*, has also appeared (Whitmore, 1995; Rietveld, 1995; Duquet et al., 2001; Liu, 2002). In this method, a linear time delay, based on the distance from the shotpoints from some reference location, is used to combine different shot records. The surface data are transformed from the response to point sources to the response to linear or planar sources.

In this paper, we review our formulation of delayed-shot migration for 3D prestack imaging of marine data, discuss its realistic cost impact and illustrate its applicability with a synthetic data example.

Delayed-shot migration versus common-shot migration

Common-shot migration is performed on individual common-shot records, and the individually migrated records are typically stacked to form the final image of the Earth's subsurface. Each migration is performed by using the wave equation to downward continue both the wavefield recorded at the receiver locations and the wavefield initiated at the shotpoint, and combining these downward-continued wavefields with an imaging condition. Since the shotpoint is localized in space, it acts (in 3D) as a point source, emitting waves that are spherical, at least near the shotpoint. Although a localized source distribution near the Earth's surface can be considered as a point source, numerical simulation of 2-D wave behavior using finite difference methods typically contains the tacit assumption that the source is a line source in 3D, with no spreading in the out-of-plane direction. Then it is possible to perform a decomposition of the recorded data into plane-wave components by using some variant of slant stack processing. This involves applying a linear time delay to each shot record (Figure 1). Specifically, each receiver gather is transformed into plane waves as:

$$u(x, p, z = 0; \omega) = \int U(x, x_s, z = 0; \omega) e^{i\omega p x_s} dx_s,$$

and its corresponding plane wave source is $d(x, p, z = 0; \omega) = e^{i\omega p x}$. If this is performed in the frequency domain, the slant stack can be viewed as a Fourier transform, with ωp replacing the spatial frequency. Viewed as a discrete Fourier transform, the slant stack should obey sampling rules that apply to the Fourier transform. These rules determine both the number N_p of plane-wave components and their spacing Δp . In particular, N_p should approximate N_{x_s} , the number of traces in a common-receiver record, for unambiguous representation of the final image.

Our motivation for performing delayed-shot migration is to improve the efficiency of wave-equation migration. To this end, we compare the costs of 2-D plane-wave migration and 2-D common-shot migration. Given N_{x_s} shot records in a sail line with shot and receiver spacings Δx_s and Δx_r , respectively, and the length L_{ap} of the full migration

Delayed-shot 3D prestack depth migration

aperture, the computational cost C_{cs} of common-shot migration is proportional to the number of x -grid points within the aperture $L_{ap}/\Delta x_r$, multiplied by N_{xs} , i.e.

$$C_{cs} = KN_{xs}L_{ap}/\Delta x_r, \quad (1)$$

where K is a unit computation constant, representing the average number of arithmetic operations on each migration grid point times the number of migration depths. For plane-wave migration, we have N_p records; all have the entire line for the migration aperture, with size $N_{xs}\Delta x_s/\Delta x_r$. Since the number of operations per grid point is the same as for common-shot migration, constant K has the same value as for common-shot migration, and the computational cost C_{pw} of plane-wave migration is

$$C_{pw} = KN_p N_{xs} \Delta x_s / \Delta x_r. \quad (2)$$

The ratio of Eqs. (1) and (2) gives the speedup of plane-wave migration over common-shot migration:

$$R_{2D} = \frac{C_{cs}}{C_{pw}} = \frac{L_{ap}}{N_p \Delta x_s}. \quad (3)$$

For marine data processing, typical values are $L_{ap} = 15\text{km}$, $N_p = 100$ and $\Delta x_s = 75\text{m}$ (Figure 2).

Then Eq. (3) gives a speedup ratio of 2, indicating that 2-D plane-wave migration will be roughly twice as fast as 2-D common-shot migration. Counterintuitively, this speedup ratio does not explicitly depend on the number of shots.

3D provides more degrees of freedom for the slant stack, and allows more possibilities for delayed-shot migration, than does 2-D. For example, we might choose to apply a linear delay to each shot record, exactly as in 2-D. Although the slant-stack (τ - p_x) processing for this case is similar to the 2-D processing, the result is a set of N_{px} records that are the responses not to *plane-wave* excitation, but rather to *linear* excitation along a sail line. In the subsurface, this source wavefield takes the shape of a cone, distorted by the velocity variations (Whitmore, 1995). Alternatively, we can apply a full plane-wave (τ - p_x , p_y) decomposition, obtaining $N_{px}N_{py}$ records that are the responses to plane waves that tilt with respect to both the x - and y -axes. In the former case (linear source), the speedup of delayed-shot migration over common-shot migration is exactly the same as Eq. (3), namely

$$R_{3D,linear} = \frac{L_{apx}}{N_{px}\Delta x_s}, \quad (4)$$

where L_{apx} is the size of the aperture of common-shot migration in the x -direction, i.e., the sail line direction. In the latter case (plane-wave source), the speedup factor needs to be modified to account for the speedup, if any, in the y -direction. This speedup factor is

$$R_{3D,planar} = \frac{L_{apx}}{N_{px}\Delta x_s} \frac{L_{apy}}{N_{py}\Delta y_s}, \quad (5)$$

where L_{apy} , N_{py} and Δy_s correspond to quantities L_{apx} , N_{px} and Δx_s in the y -direction. For 3D marine data, the distance Δy_s between adjacent shot lines is usually considerably larger than Δx_s , the shot spacing along one sail line. Typical values are $\Delta x_s = 75\text{m}$ and $\Delta y_s = 160\text{m}$. Using these values, and setting $L_{apx} = L_{apy} = 15\text{km}$ and $N_{px} = N_{py} = 100$, we find the speedup ratio for 3D line-source migration is 2 (as in 2-D), while the speedup ratio for 3D plane-source migration is 1.875.

It is possible to improve these speedup ratios, giving linear-source and planar-source migration almost arbitrarily high speedups over common-shot migration, in both 2-D and 3D, simply by reducing N_{px} and/or N_{py} . As mentioned

above, however, we must be prepared to pay a certain price for doing this, either by reducing the largest p -value (losing steep dips) or, more insidiously, by allowing Fourier transform artifacts to be introduced into the image by increasing the spacing Δp . A certain amount of Fourier transform-related noise might not degrade the final stack, but it is difficult to estimate in advance how much of this noise can be tolerated in any of the individual migrated records.

Likewise, it is possible to speed up the process of common-shot migration, simply by reducing the number of records to be migrated. If we do this by decimating shots, we must be prepared to provide an image whose near-surface is at least somewhat degraded.

As in common-shot migration (Zhang, et al., 2002, 2003), some true amplitude conditions need to be applied during the delayed-shot migration to ensure the migrated amplitude on each p -section $R_p(\vec{x})$ has some geophysical meanings. We also need to stack all the migrated p -sections to obtain an overall picture of subsurface structures. However, the amplitude on the stacked migration section is usually unbalanced. This is mainly due to the acquisition limitations (irregular surface shot coverage, finite cable length and the missing of near offsets, etc.) and the velocity complexity. A popular way to overcome this problem is illumination compensation, in which a cost-effective illumination factor $W(\vec{x})$ is calculated and then applied to the stacked image

$$R(\vec{x}) = \sum_p R_p(\vec{x}) / W(\vec{x}). \quad (6)$$

For delayed-shot migration, the illumination from the sources is similar to that from the receivers. So we only need to calculate the illumination factor from the source

Delayed-shot 3D prestack depth migration

side. Similar to the type 2 common-shot formulation derived in Plessix and Mulder (2002), in delayed-shot migration we choose

$$W(\bar{x}) = \sum_p \left(\sum_{\omega} |G(\bar{x}, p; \omega)|^2 \right)^2 \quad (7)$$

where $G(\bar{x}, p; \omega)$ is the Green function corresponding to a single linear source or a plane-wave source.

Examples

Figure 3 compares an image from delayed-shot migration with one from common-shot migration. The receiver station interval is 75 ft and the shot interval is 150 ft. The cable length is 26025 ft. The image in Fig. 3b is a stack of images from 121 p -values with surface incidence angle ranging from -52° to 34° . The image is slightly noisier than the one from common-shot migration, but all structures are well imaged by both migrations. We have also migrated this data set using 241 p -values, with a result essentially identical to the common-shot migrated image. As sampling theory predicts, the noise level in the image progressively increases as we use fewer p -values. To obtain a more amplitude balanced image, we calculate illumination map (Fig. 4a) according to formulation (7) and apply it to the stacked section, the result is shown in Fig. 4b. Figure 5 shows angle-domain common image gathers (ADCIG's) from common-shot migration and delayed-shot migration, respectively. These angle gathers can be used for updating the velocity field or for AVO/AVA analysis. Unlike common-shot migration, whose ADCIG's are indexed by *subsurface* incidence angle, the angle from delayed-shot migration is the *surface* incidence angle. Producing angle gathers from delayed-shot migration is far more cost-effective than from common-shot migration since it requires no additional computation or network communication. We see this as a very important advantage of delayed-shot migration.

Conclusions

We have reviewed the methodology for performing delayed-shot migration in 2-D based on slant-stacking

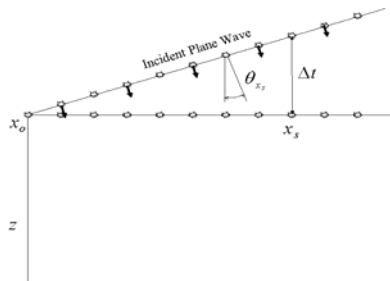


Figure 1. Plane wave schematic.

common receiver gathers along the sail line direction. We compared two alternatives for extending this to 3D, namely by forming linear slant-stack sources as in 2-D or applying a full plane-wave decomposition in both x - and y -directions. Delayed-shot migration of the Sigsbee2A synthetic data set, with carefully chosen slant-stack parameters, has produced an image comparable to a common-shot migrated image.

References

- Duquet, B., Lailly, P. and Ehinger, A., 2001, 3D Plane wave migration of streamer data, 71st Ann. Mtg., Soc. Expl. Geophy.
- Liu, F., Stolt, R. H., Hanson, D. W. and Day, R. S., 2002, Plane wave source composition: an accurate phase encoding scheme for prestack migration, 72nd Ann. Mtg., Soc. Expl. Geophys.
- Plessix, R. E. and Mulder, W., 2002, Amplitude-preserving finite-difference migration based on a least-squares formulation in the frequency domain, 72nd Ann. Mtg., Soc. Expl. Geophys., 1212-1215.
- Rietveld, W. E. A., 1995, Controlled illumination of prestack seismic migration, Ph.D. thesis, Delft University of Technology.
- Romero, L. A., Ghiglia, D. C., Ober, C.C. and Morton, S A., 2000, Phase encoding of shot records in prestack migration, Geophysics, 65, 426-436.
- Whitmore, N. D., 1995, An imaging hierarchy for common angle plane wave seismograms, Ph.D. thesis, University of Tulsa.
- Zhang, Y., Sun, J., Gray, S., Nottfors, C., and Bleistein, N., 2001, Towards accurate amplitudes for one-way wavefield extrapolation of 3D common shot records, 71st Ann. Mtg., Soc. Expl. Geophy. (Workshop).
- Zhang, Y., Zhang, G., and Bleistein, N., 2002, Theory of true amplitude common-shot migration, 72nd Ann. Mtg., Soc. Expl. Geophys..

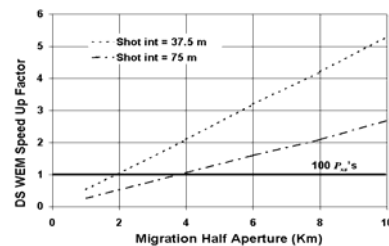


Figure 2. The speedup ratio for delayed-shot migration versus common shot migration.

Delayed-shot 3D prestack depth migration

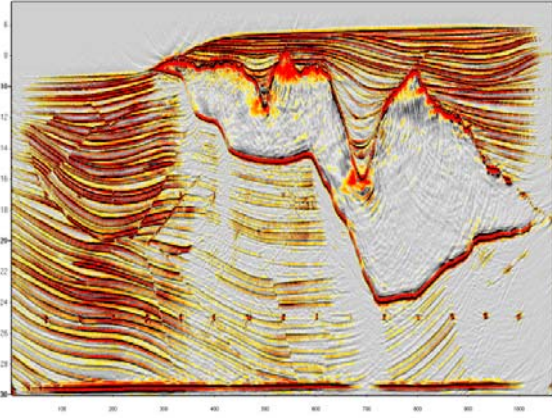


Figure 3a. Common-shot migration.

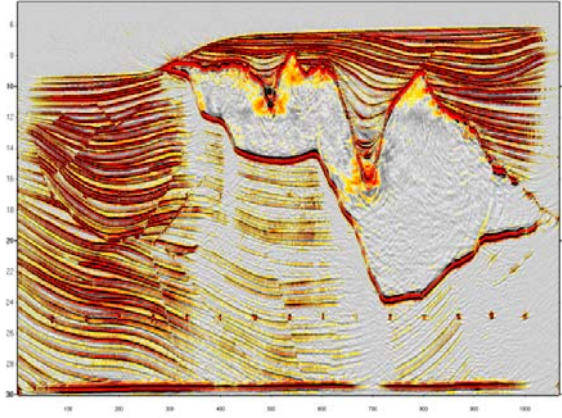


Figure 3b. Delayed-shot migration with 121 p 's.

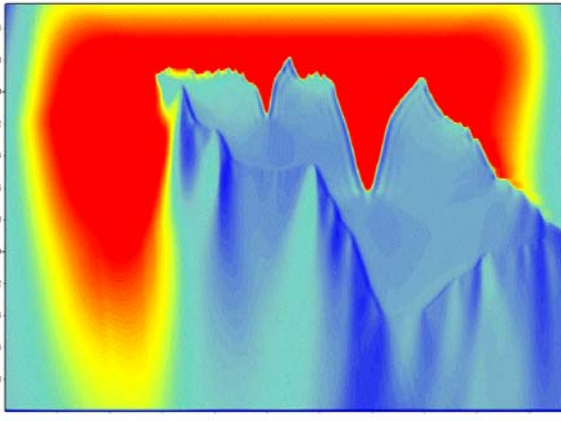


Figure 4a. Illumination map of delayed-shot migration.

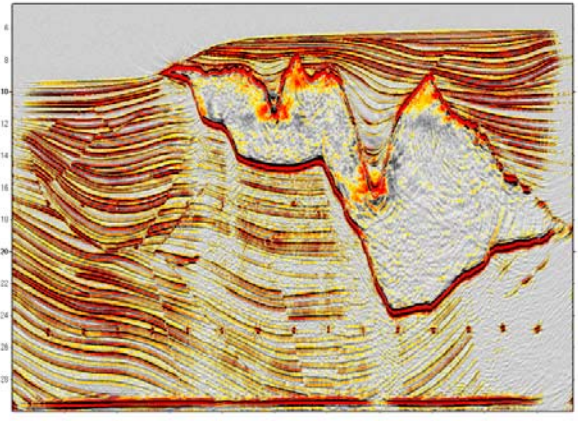


Figure 3b. Delayed-shot migration (121 p 's) with illumination compensation.

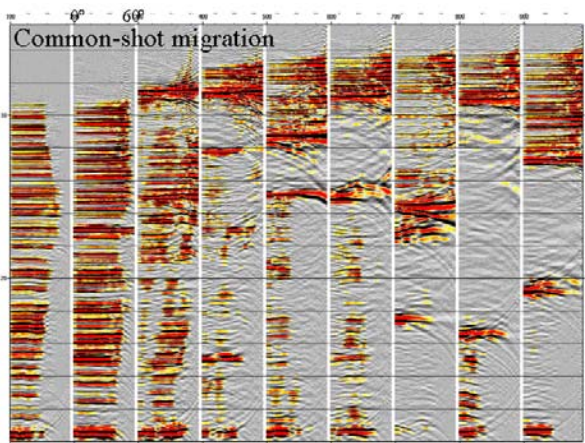


Figure 4a. Common-image-gathers indexed by subsurface opening angle from common-shot migration. The angle range is from 0° to 60° .

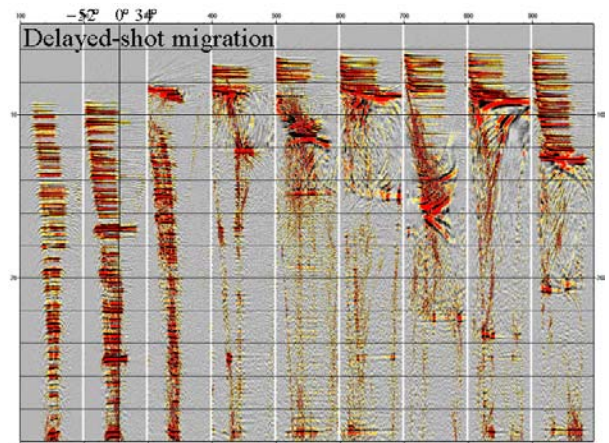


Figure 4b. Common-image-gathers indexed by surface incidence angle from delayed-shot migration. The angle range is from -52° to 34° .